



Electromagnetic interference shielding properties of ferrocene-based polypyrrole/carbon material composites

Ahsan Nazir¹ · Haojie Yu¹ · Li Wang¹ · Yang He² · Quan Chen² · Bilal Ul Amin¹ · Di Shen¹

Received: 19 December 2019 / Accepted: 19 August 2020 / Published online: 28 August 2020
© Springer-Verlag GmbH Germany, part of Springer Nature 2020

Abstract

Ferrocene-based polypyrrole (PPyFc) composites containing multi-walled carbon nanotube (MWCNT), reduced graphene oxide (RGO) and carbon black (CB) have been prepared by chemical oxidative polymerization. The prepared PPyFc/MWCNT, PPyFc/RGO and PPyFc/CB composites have been characterized by SEM, TEM, FTIR, XRD, XPS and TGA. Electrical conductivity of the PPyFc/MWCNT, PPyFc/RGO and PPyFc/CB composites has been tested by a typical four-probe method. Furthermore, the electromagnetic interference shielding effectiveness (EMI SE) of the PPyFc/CB, PPyFc/RGO and PPyFc/MWCNT composites has been measured through a coaxial method in the S-band frequency range. The EMI SE achieved for PPyFc/CB, PPyFc/RGO and PPyFc/MWCNT composites was -11.08 dB, -11.44 dB and -23.74 dB, respectively.

Keywords Ferrocene-based polypyrrole · Composites · Electromagnetic interference shielding properties

1 Introduction

The extensive use of electronic and communication gadgets such as laptops, tablets, cell phones, and smart television, generates severe electromagnetic (EM) radiation [1]. The EM radiation has a harmful effect on the environment and performance of commercial, civil, military appliances [2–4]. Moreover, the continued EM radiations may also interfere with the operation of sensitive electronic equipment [5–7]. These problems can be reduced and can save society and precious electronic equipment from such a hazardous effect of EM radiations using highly effective shielding materials [8]. To deal with these critical problems, traditional metal-based shielding materials are by far the most common materials for electromagnetic interference (EMI) shielding [9],

owing to their excellent electrical conductivity. However, they suffered from a lot of disadvantages such as expensive processing, high mass density and complexity in manufacturing techniques [10]. On the other hand, most common eco-friendly polymer-based composites containing conductive fillers have gained enormous attention as EMI shielding materials from both the scientific community and industry [11], because of their remarkable properties like easy-to-fabricate, excellent electrical, thermal and EMI shielding properties [12]. These properties are essential to provide promising applications of EMI shielding field especially in the areas of electronics, aerospace, aircraft, wearable devices and automobiles, etc. [13–16].

In recent years, most of the researchers have focused on the conductive polymer composites containing carbon materials such as carbon nanotubes (CNTs) [17–23], reduced graphene oxide (RGO) [24–28] and carbon black (CB) [29, 30] are the most used materials within the insulating and conductive polymer and have been studied for the applications of EMI shielding [31]. Among other conductive polymers, polypyrrole (PPy) has attracted a great deal of interest owing to its good electrical conductivity, easy synthesis, porous nature and environmental stability [32]. Moreover, PPy has been used in various applications such as batteries, electrochromic devices, supercapacitors, anti-corrosive materials, sensors and electrostatic charge

✉ Haojie Yu
hjyu@zju.edu.cn

✉ Li Wang
opl_wl@dial.zju.edu.cn

¹ State Key Laboratory of Chemical Engineering, College of Chemical and Biological Engineering, Zhejiang University, Hangzhou 310027, People's Republic of China

² Bull Group Co., Ltd., No. 88 Rixian North Road, CiDong Binhai District, Cixi City, Ningbo 315318, Zhejiang, People's Republic of China

dissipation [33]. Interestingly, due to its remarkable properties, PPy has gained enormous attention and has been widely used as EMI shielding materials, nowadays [34, 35].

Organometallic compounds have also gained considerable interest due to their attractive properties such as high chemical, magnetic, and better redox activity [36, 37]. Even so, ferrocene is an organometallic compound which contains the iron present between two cyclopentadienyl rings. In addition, ferrocene-based polymers are hot areas of research from its discovery until now [38, 39]. In our previous work, we fabricated ferrocene-based polythiophene (PTFc) composites containing multi-walled carbon nanotubes (MWCNTs), RGO and CB, respectively, and investigated their EMI shielding properties. In that work, we provided a simple method to fabricate good electrical conductive and EMI shielding materials. In the present work, we introduced polypyrrole (PPy) for further improvement of EMI shielding property and it is expected that introducing PPy can enhance the EMI shielding property.

For this purpose, ferrocene-based polypyrrole (PPyFc)/carbon material composites have been prepared by chemical oxidative polymerization, respectively. We introduced PPyFc which is useful for EMI SE because PPyFc contains the properties of polypyrrole and ferrocene groups which have the ability to transfer electron on the carbon materials and excellent redox properties, respectively. PPyFc may promote conductive properties of the composites which are essential for EMI shielding performance. This kind of polymer composites has potential applications in a number of important areas such as satellite communication, wireless networking devices and home-based consumer electronics. The EMI shielding property of the composites has been measured through the coaxial method in the S-band frequency range.

2 Experimental section

2.1 Materials

Dichloromethane (DCM), chloroform (CHCl_3), sodium carbonate (Na_2CO_3), ferrocene carboxylic acid, ethylenediaminetetraacetic acid (EDTA) and anhydrous iron trichloride (FeCl_3) were purchased from Sinopharm Chemical Reagent Co. Ltd. *N*-(2-Cyanoethyl) pyrrole was supplied by J&K Scientific. Co. Ltd. MWCNTs were obtained from Sigma-Aldrich. Natural graphite powder was provided by Alfa Aesar. CB was provided by the Chemical Industry (China). CHCl_3 was used after drying with 4A molecular sieves. DCM was distilled in the presence of calcium hydride. Other chemicals were used directly as received.

2.2 Synthesis of 1-(3-aminopropyl) pyrrole ferrocene (PyFc)

Firstly, 1-(3-aminopropyl) pyrrole (Py) was synthesized by catalytic reduction of *N*-(2-cyanoethyl) pyrrole according to the previously reported procedure [40]. Subsequently, PyFc was prepared by the reaction between ferrocene carbonyl chloride and Py. Briefly, Py (5.9568 g, 48.09 mmol) was taken in a flask and dissolved in freshly distilled DCM (20 ml). Afterward, ferrocene carbonyl chloride solution (12.0010 g, 48.09 mmol) prepared in freshly distilled DCM (60 ml) was added dropwise to the Py solution. Pyridine (4.2 ml, 52.89 mmol) was added to the previous solution. Then the resulting solution was refluxed for 30 h. The resulting solution was washed by a saturated solution of 5% Na_2CO_3 (200 ml \times 3 times) and distilled water (200 ml \times 3 times), respectively. The organic layer was dried with MgSO_4 overnight, filtered and the solvent was evaporated. The product (PyFc) was dried under vacuum oven at 40 °C.

2.3 Synthesis of ferrocene-based polypyrrole (PPyFc)

PyFc was polymerized to prepare PPyFc according to the reported method [41]. In a typical procedure, anhydrous FeCl_3 (1.9269 g, 11.88 mmol) was added in a flask and then was dried under vacuum. Afterward, 70 ml of CHCl_3 was added to the dried FeCl_3 . The obtained mixture was vigorously stirred to get a homogenous suspension. In another flask, the monomer PyFc (0.9997 g, 2.97 mmol) was dissolved in 30 ml of CHCl_3 . The PyFc solution was added slowly to the obtained FeCl_3 suspension and the resulting mixture was stirred for 8 h at 25 °C. The obtained mixture was concentrated and then the concentrated mixture was precipitated in methanol. The precipitated solid was collected through centrifugation. The obtained solid was added to 20 ml of CHCl_3 and then the resulting mixture was refluxed with 50 ml of 14.7 M ammonia solution for 1 h. Afterward, separate the organic layer, washed with 50 ml of 14.7 M ammonia solution, 100 ml of 0.5 M EDTA solution and distilled water, respectively. The solvent was evaporated and the product (PPyFc) was dried under vacuum oven at 40 °C.

2.4 Preparation of PPyFc/carbon material composites

The oxidative polymerization has been used to prepare PPyFc/carbon material composites. In a typical procedure, anhydrous FeCl_3 (1.9274 g, 11.88 mmol) was added in a flask and then was dried under vacuum. Afterward, 70 ml of CHCl_3 was added to the dried FeCl_3 . The obtained mixture

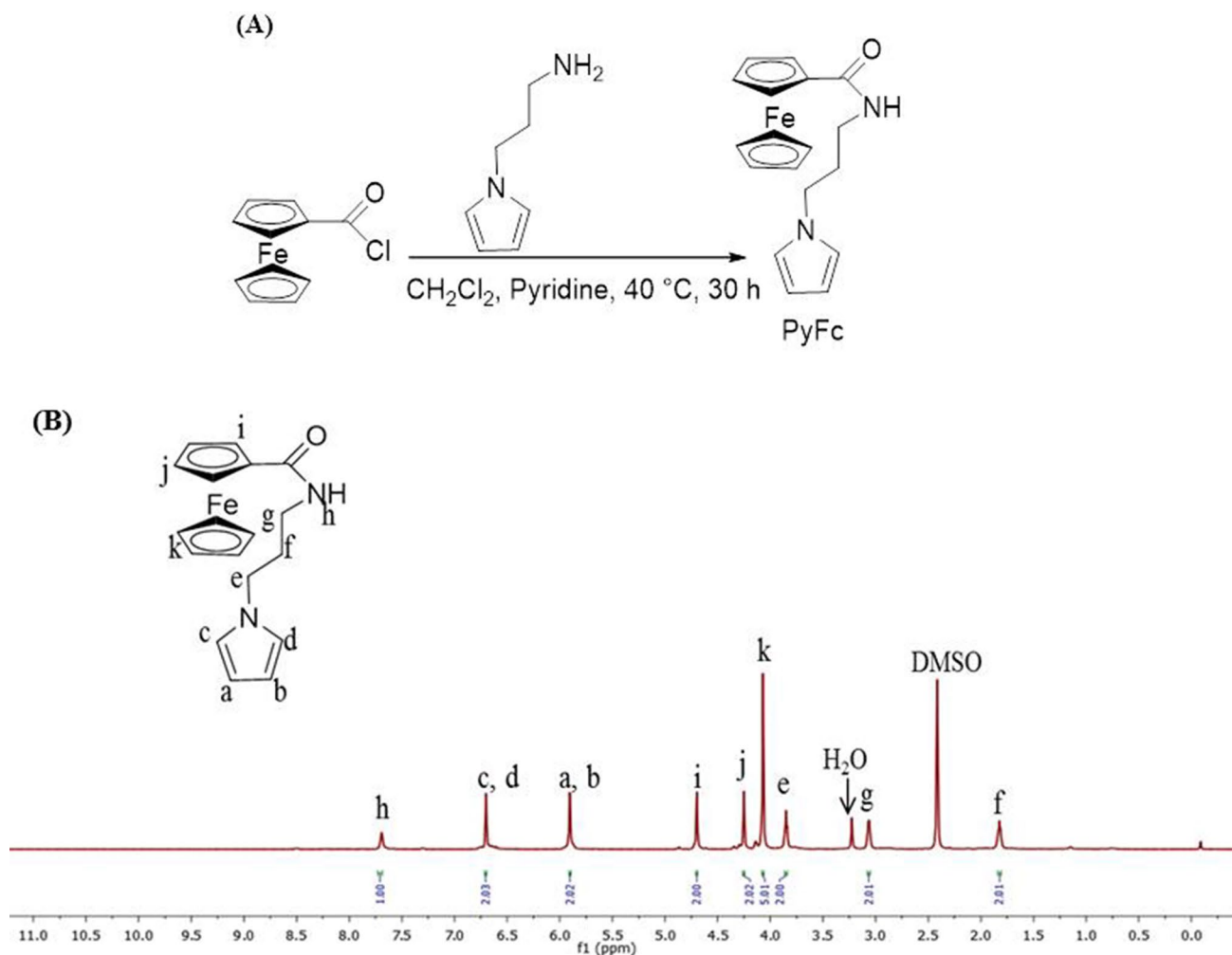


Fig. 1 a Schematic illustration of the synthesis of PyFc and b ^1H NMR spectrum of PyFc

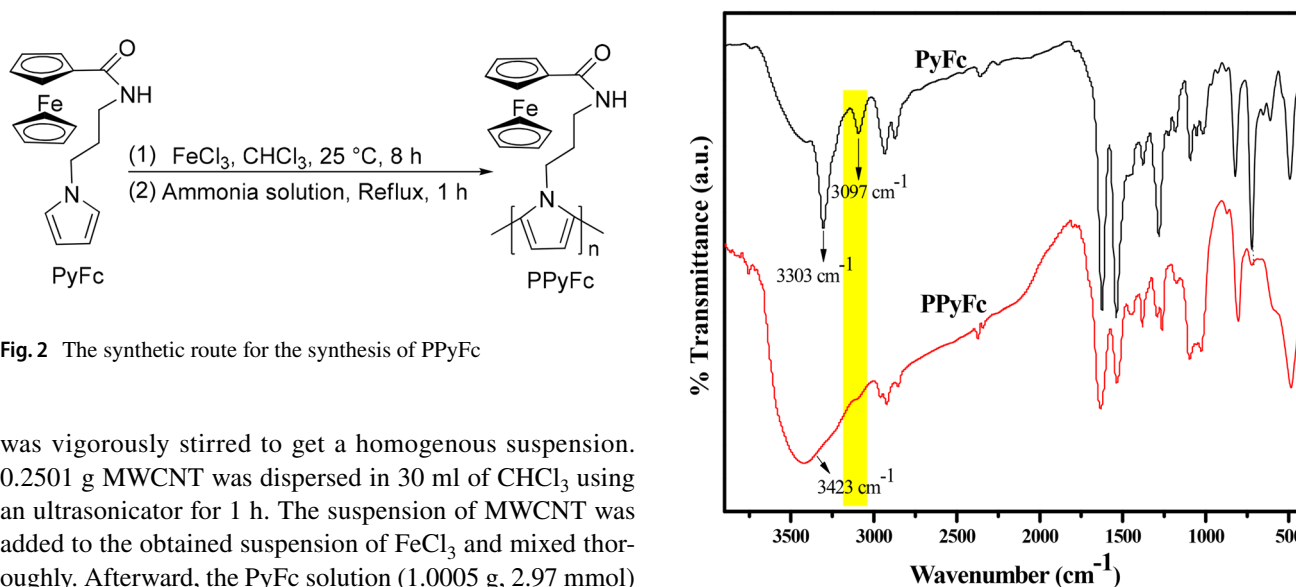


Fig. 2 The synthetic route for the synthesis of PPyFc

was vigorously stirred to get a homogenous suspension. 0.2501 g MWCNT was dispersed in 30 ml of CHCl_3 using an ultrasonicator for 1 h. The suspension of MWCNT was added to the obtained suspension of FeCl_3 and mixed thoroughly. Afterward, the PyFc solution (1.0005 g, 2.97 mmol) prepared in 30 ml of CHCl_3 was added slowly to the obtained FeCl_3 and MWCNT suspension and the resulting mixture

Fig. 3 FTIR spectra of PyFc and PPyFc

was stirred for 8 h at 25 °C. The obtained mixture was concentrated and then the concentrated mixture was precipitated in methanol. The precipitated solid was collected through centrifugation. The obtained solid was added to 20 ml of CHCl_3 and then the resulting mixture was refluxed with 50 ml of 14.7 M ammonia solution for 1 h. After completing the reflux, the precipitates were separated from the resulting mixture through filtration. Then, the filtered solid was washed with 50 ml of 14.7 M ammonia solution, 100 ml

of 0.5 M EDTA solution and distilled water, respectively. Finally, the powdery composite was dried under vacuum oven at 40 °C. In the overall experiment, the mass ratio of MWCNT and PyFc was chosen 1:4, and the molar ratio of FeCl_3 and PyFc was kept at 4:1. In the above similar process, PPyFc composites with RGO and CB have also been prepared and the composites have been abbreviated as PPyFc/MWCNT, PPyFc/RGO and PPyFc/CB, respectively.

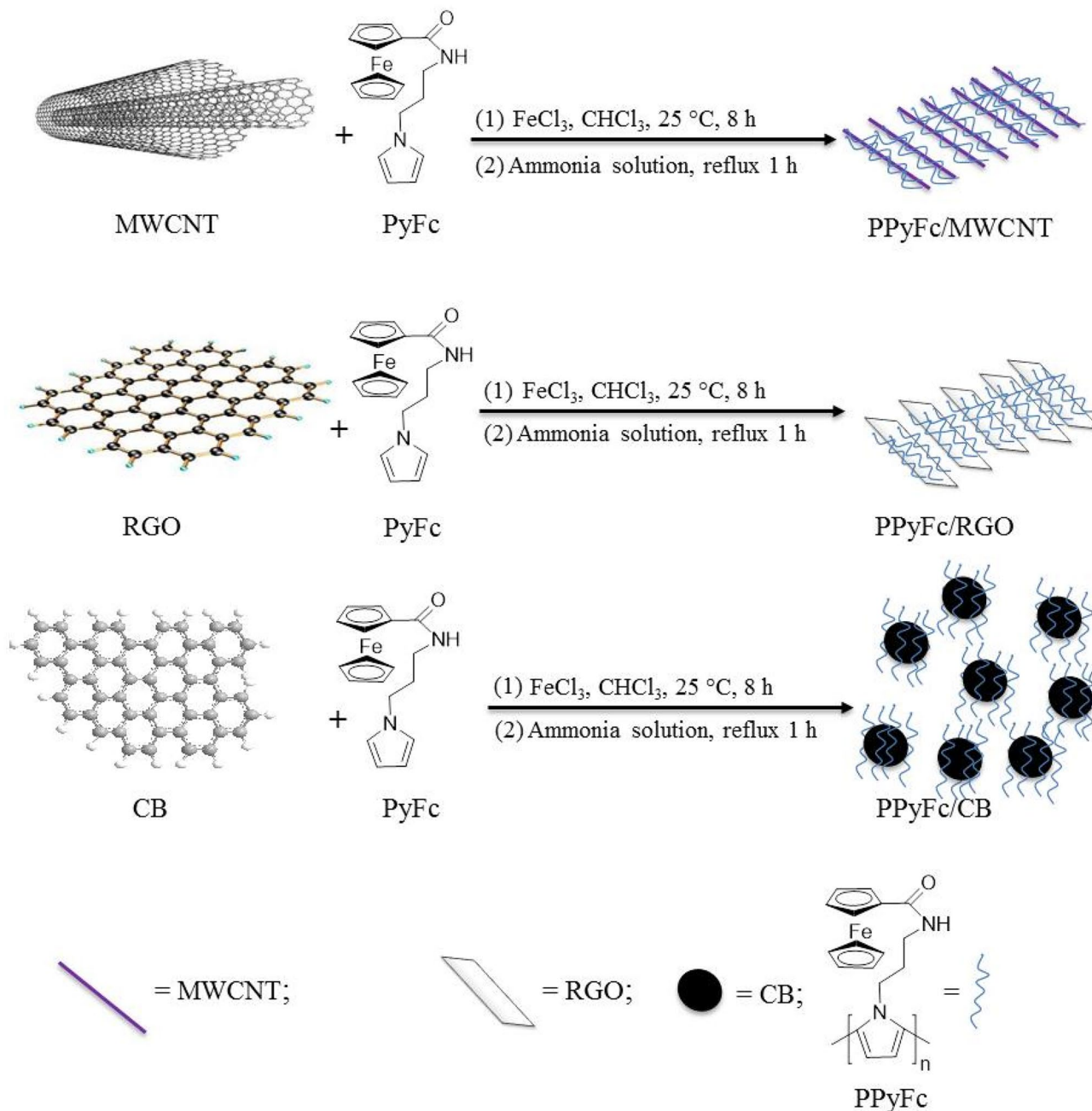


Fig. 4 Schematic illustration of the preparation of PPyFc/carbon material composites

2.5 Characterization

The ^1H NMR spectrum of the synthesized monomer was obtained from a Bruker Advance NMR spectrometer (600 MHz, Model DMX-400). The surface morphology of the samples was observed using a scanning electron microscope (Model JEOL-6700F, SEM) and a transmission electron microscope (Model JEOL-1200EX, TEM). Fourier transform infrared (FTIR), X-ray diffraction (XRD) and X-ray photoelectron spectroscopy (XPS) spectra were studied using a Nicolet-5700 IR spectrometer, XPert PRO ($\text{CuK}\alpha$, $\lambda = 1.54 \text{ \AA}$), VG ESCALAB MKII XPS system, respectively. Thermogravimetric analysis (TGA) was performed using TA-Q500 (Mettler-Toledo) at a heating rate of $10 \text{ }^\circ\text{C}/\text{min}$ under a nitrogen atmosphere in the range of $50\text{--}800 \text{ }^\circ\text{C}$. The electrical conductivity was tested by a SB100A/2 four-probe conductivity meter (Shanghai Qianfeng Electronic Instrument Co. Ltd. China). For conductivity measurement, the powder of the samples was pressed using a manual hydraulic press machine and the thin film was prepared. The EMI SE of the samples was measured using a vector network analyzer (Agilent, E5071C) through the coaxial method. For EM measurement, the powder samples with 50 wt% were uniformly mixed with paraffin. Coaxial specimens were prepared in toroid-shaped samples with an inner diameter of 3.04 mm, the outer diameter of 7.0 mm and the thickness of about 3.0 mm.

3 Results and discussion

3.1 Synthesis of PyFc and PPyFc

PyFc was successfully synthesized by the amidation reaction of ferrocene carbonyl chloride and Py as shown in Fig. 1a. The structure of PyFc was confirmed by ^1H NMR as shown in Fig. 1b. It shows peaks with following chemical shifts (DMSO, δ in ppm): 1.81–1.84 (2H, H_f), 3.05–3.08 (2H, H_g), 3.85–3.88 (2H, H_e), 4.07–4.10 (5H, H_k), 4.25–4.28 (2H, H_j), 4.69–4.72 (2H, H_i), 5.90–5.93 (2H, $\text{H}_{a, b}$), 6.70–6.73 (2H, $\text{H}_{c, d}$) and 7.69–7.72 (1H, H_b) ppm.

PPyFc was synthesized through oxidative polymerization of PyFc with anhydrous FeCl_3 . The synthetic route of PPyFc is given in Fig. 2. The structure of PPyFc was confirmed by FTIR. In the PyFc spectrum (Fig. 3), a broad peak appears at 3303 cm^{-1} which is due to the N–H stretching vibration. The peak at 3097 cm^{-1} is assigned to the $\text{C}_\alpha\text{--H}$ stretching vibration of the pyrrole ring. But after polymerization of PyFc, the N–H stretching vibration peak observed at 3423 cm^{-1} , whereas the characteristic peak at 3097 cm^{-1} for $\text{C}_\alpha\text{--H}$ stretching vibration of the pyrrole ring is completely disappeared. The disappearance of a $\text{C}_\alpha\text{--H}$ stretching vibration in the PPyFc confirmed that the

Table 1 Details of the synthesis of PPyFc, PPyFc/MWCNT, PPyFc/RGO and PPyFc/CB

Sample	Step 1		Step 2		Step 3		Step 4		Step 5		Step 6			
	FeCl_3 g	CHCl_3 ml	Carbon material g	T_1/t_1 $^\circ\text{C}/\text{h}$	CHCl_3 ml	T_2/t_2 $^\circ\text{C}/\text{h}$	T_3/t_3 $^\circ\text{C}/\text{min}$	PyFc g	CHCl_3 ml	T_4/t_4 $^\circ\text{C}/\text{min}$	FeCl_3 : PyFc mmol: mmol	T_5/t_5 $^\circ\text{C}/\text{h}$	Ammonia solution ^a ml	T_6/t_6 $^\circ\text{C}/\text{h}$
PPyFc	1.9269	11.88	–	RT/0.5	–	–	RT/10	0.9997	2.97	RT/10	4:1	25/8	50	40/1
PPyFc/MWCNT	1.9274	11.88	0.2501 (MWCNT)	RT/0.5	30	RT/1	RT/10	1.0005	2.97	RT/10	4:1	25/8	50	40/1
PPyFc/RGO	1.9272	11.88	0.2529 (RGO)	RT/0.5	30	RT/1	RT/10	1.0012	2.97	RT/10	4:1	25/8	50	40/1
PPyFc/CB	1.9280	11.88	0.2526 (CB)	RT/0.5	30	RT/1	RT/10	1.0008	2.97	RT/10	4:1	25/8	50	40/1

^aThe concentration of ammonia solution is 14.7 M

polymerization has occurred on an α position of the pyrrole ring [42, 43]. The rest of the characteristic peaks of PyFc and PPyFc are almost similar.

3.2 Preparation of PPyFc/carbon material composites

The PPyFc/MWCNT, PPyFc/RGO and PPyFc/CB composites have been prepared via oxidative polymerization. The PyFc was polymerized on the carbon materials surfaces with anhydrous FeCl_3 . Usually, in the oxidative polymerization, the monomers were oxidized forming the radical cations [44]. These radical cations adsorbed on the carbon material surface via $\pi - \pi$ stacking interactions and initiated the oxidative polymerization of PyFc. Finally, PPyFc/MWCNT, PPyFc/RGO and PPyFc/CB composites were obtained. The obtained percentage of PPyFc on carbon fillers was around 81.8% for PPyFc/MWCNT, 83.5% for PPyFc/RGO and

84.4% for PPyFc/CB. The schematic illustration of the preparation of PPyFc/carbon material composites as depicted in Fig. 4. The synthetic details are presented in Table 1.

3.3 Characterization of PPyFc and PPyFc/carbon material composites

The structure and morphology of the prepared samples were investigated using various characterizations. Figure 5 shows the SEM images of MWCNT, RGO, CB, PPyFc/MWCNT, PPyFc/RGO and PPyFc/CB.

Figure 5a exhibits the pristine morphology of CNT and can be observed that CNT tend to form bundles and entangled with each other. Figure 5b exhibits the random distribution of CNT throughout the PPyFc. Pristine RGO sheet shows a flake sheet with the wrinkled surface as shown in Fig. 5c. Figure 5d shows that the surface of the RGO sheet is densely covered by PPyFc. The CB looks like round-shaped

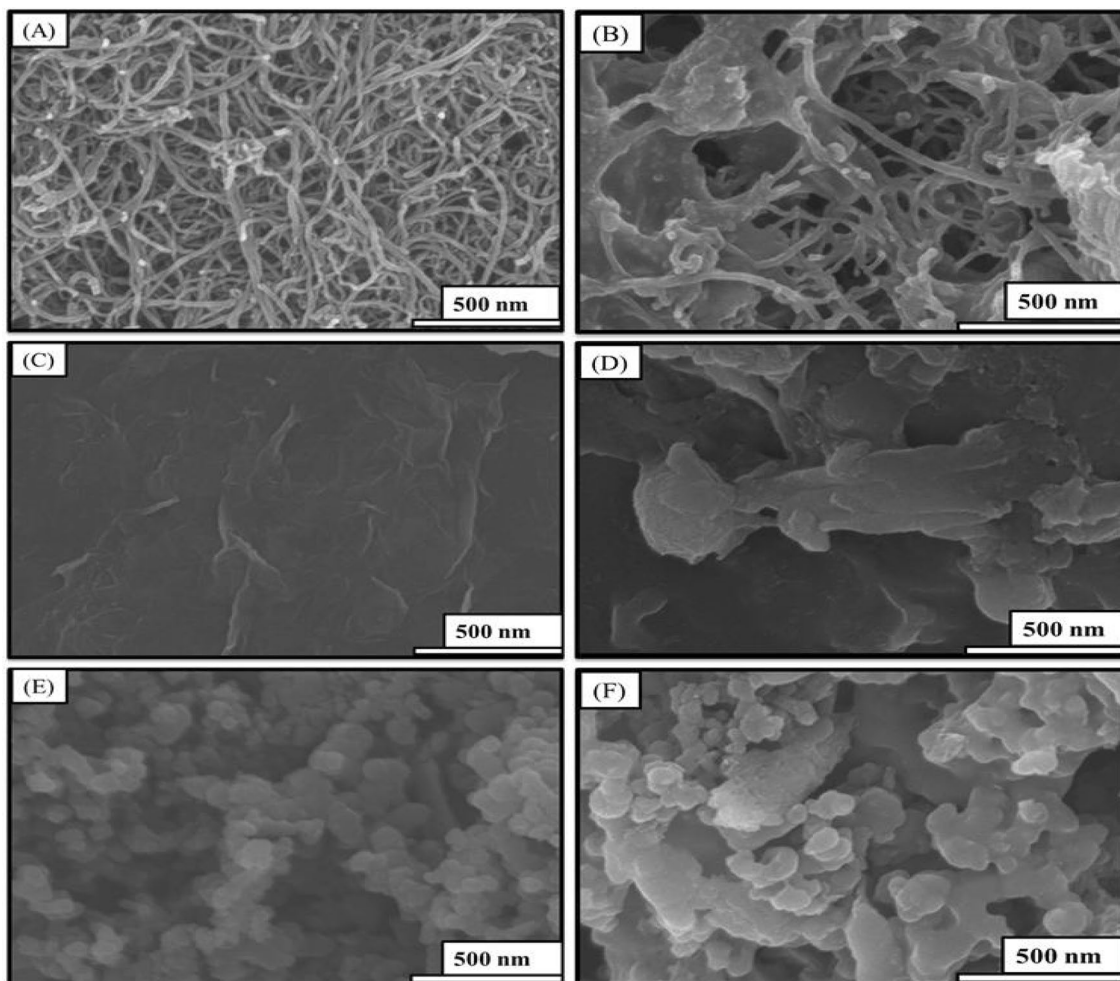


Fig. 5 SEM images of a MWCNT, b PPyFc/MWCNT, c RGO, d PPyFc/RGO, e CB and f PPyFc/CB

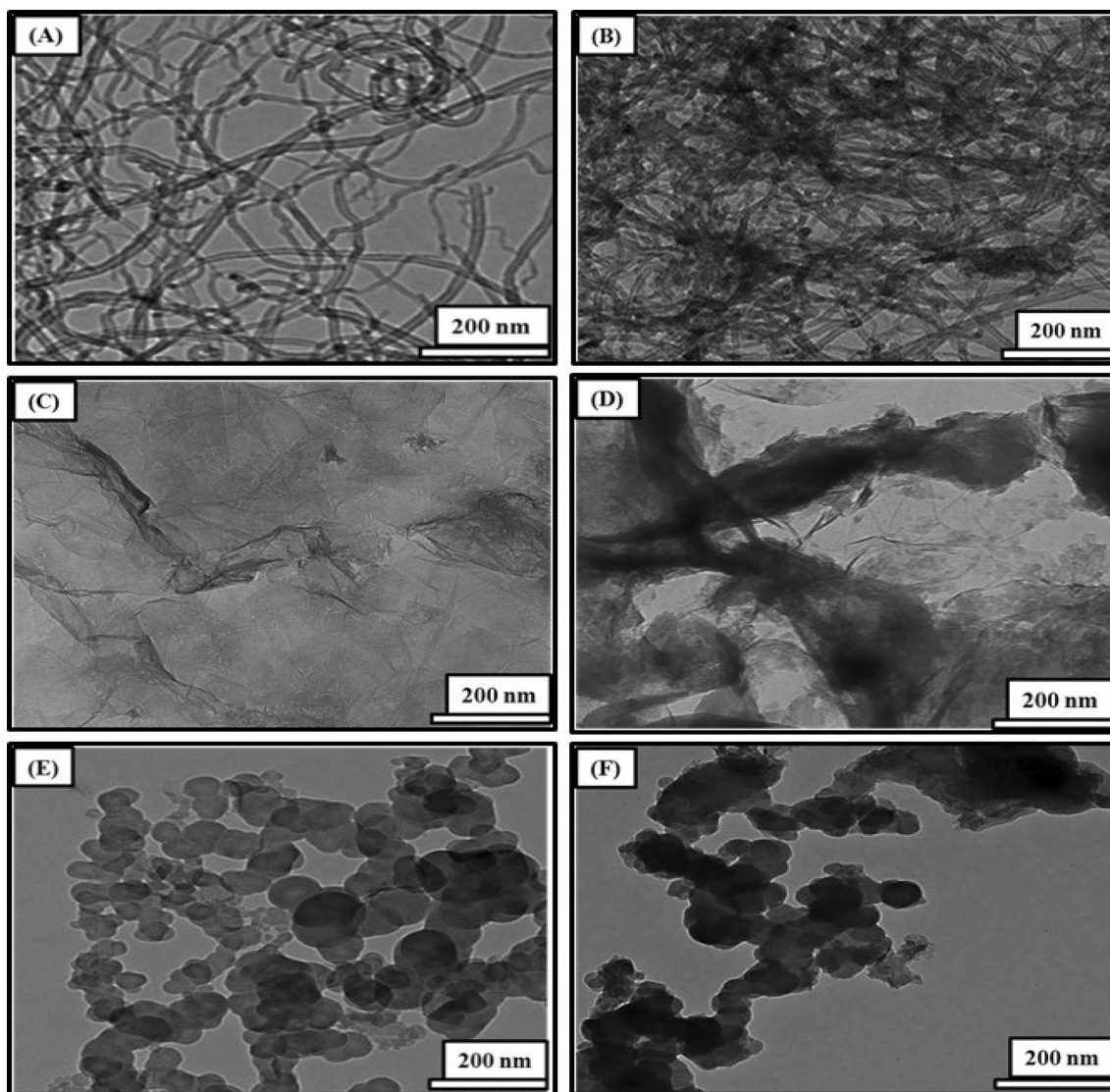


Fig. 6 TEM images of **a** MWCNT, **b** PPyFc/MWCNT, **c** RGO, **d** PPyFc/RGO, **e** CB and **f** PPyFc/CB

particles as shown in Fig. 5e. The CB particles are uniformly dispersed throughout the PPyFc as shown in Fig. 5f. SEM result of PPyFc/carbon material composites reveals that PPyFc is entrapped within the MWCNT, RGO and CB surface, respectively.

TEM images of MWCNT, RGO, CB, PPyFc/MWCNT, PPyFc/RGO and PPyFc/CB are shown in Fig. 6. The long and slender tubes of the MWCNT, highly wrinkled sheet of RGO and a small cluster of grapes of CB particles were found, as shown in Fig. 6a, c, e. While in the composites case, it can be seen in Fig. 6b, d, f exhibits the random distribution of PPyFc on MWCNT, RGO and CB surface, respectively.

The FTIR spectra of the MWCNT, RGO, CB, PPyFc, PPyFc/MWCNT, PPyFc/RGO and PPyFc/CB are shown in

Fig. 7. The FTIR spectra of carbon materials are shown in Fig. 7a, it can be seen that the characteristic peak present at 1635 cm^{-1} is attributed to C=C stretching vibration in benzenoid ring [45–47]. The FTIR spectra of PPyFc and their composites are shown in Fig. 7b. In the spectra, the broad peak located at about 3423 cm^{-1} is related to the N–H stretching vibration [48], and the characteristic peaks present at 2919 and 2847 cm^{-1} are attributed to the aromatic C–H stretching vibrations, while the peaks at 1635 and 1534 cm^{-1} are assigned to the C=C and C–C stretching vibrations of the ring, respectively [49, 50]. The peaks at 1359 and 1258 cm^{-1} are due to the stretching vibration of C–N, whereas the peaks at 1098 and 1027 cm^{-1} are caused by N–H in-plane deformation of the pyrrole unit [51]. The peaks present at 815 and 723 cm^{-1} are belonged to the C–H wagging [52, 53] and 486 cm^{-1} is

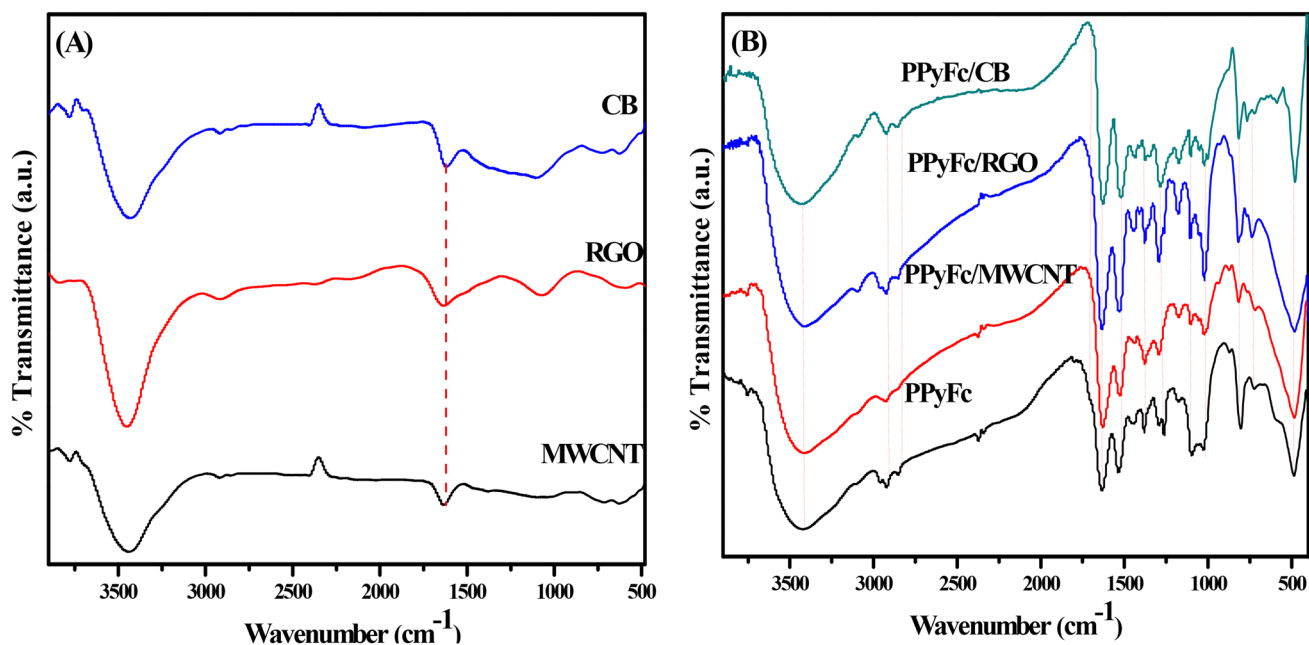


Fig. 7 FTIR spectra of a MWCNT, RGO, CB and b PPyFc, PPyFc/MWCNT, PPyFc/RGO and PPyFc/CB

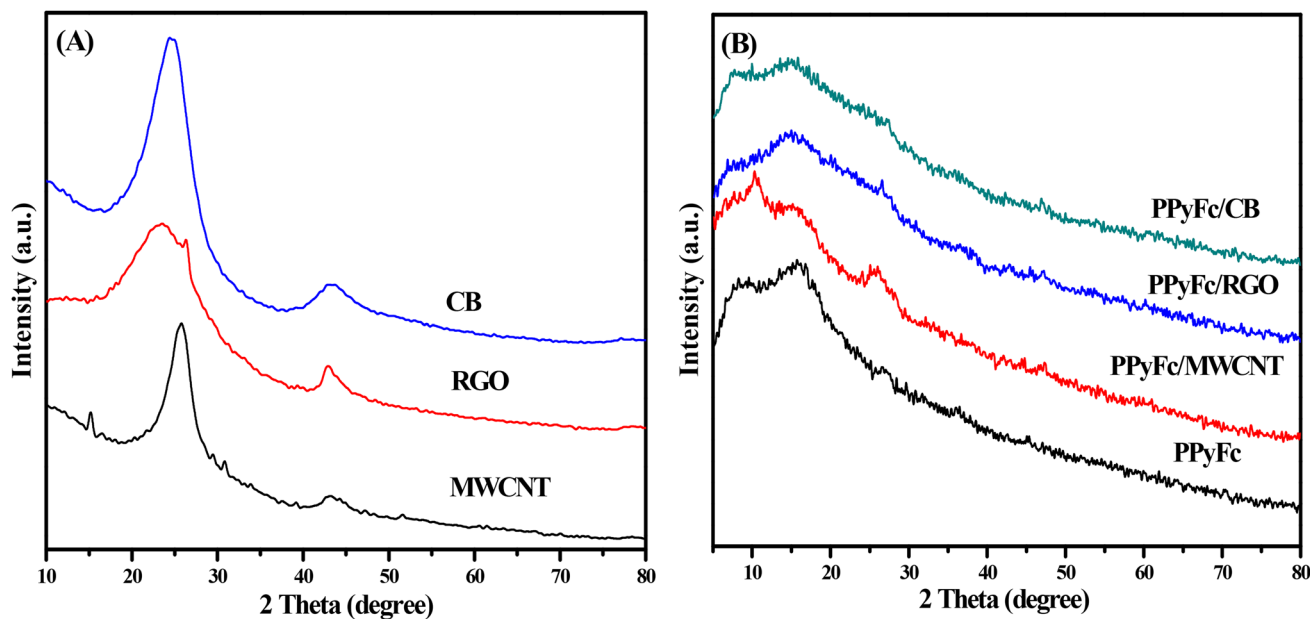


Fig. 8 XRD spectra of a MWCNT, RGO, CB and b PPyFc, PPyFc/MWCNT, PPyFc/RGO and PPyFc/CB

related to the stretching vibration of ferrocene which is present in the PPyFc [41]. The peak present at 1690 cm^{-1} is attributed to the stretching vibration of the carbonyl group of the amide. The characteristic peaks of the pure PPyFc can be seen in PPyFc/MWCNT, PPyFc/RGO and PPyFc/CB composites spectra, which indicated that PPyFc were synthesized on the MWCNT, RGO and CB surface, respectively.

The XRD spectra of the MWCNT, RGO, CB, PPyFc, PPyFc/MWCNT, PPyFc/RGO and PPyFc/CB are shown in Fig. 8. In the XRD spectra of carbon materials (Fig. 8a), the two main diffraction peaks located at around 24° and 42° [54–56]. Whereas, the broad diffraction peaks of PPyFc appeared at 8.45° and 16.73° , which shows its amorphous nature [57]. As shown in Fig. 8b, the diffraction peaks present in PPyFc have also been observed in their composites,

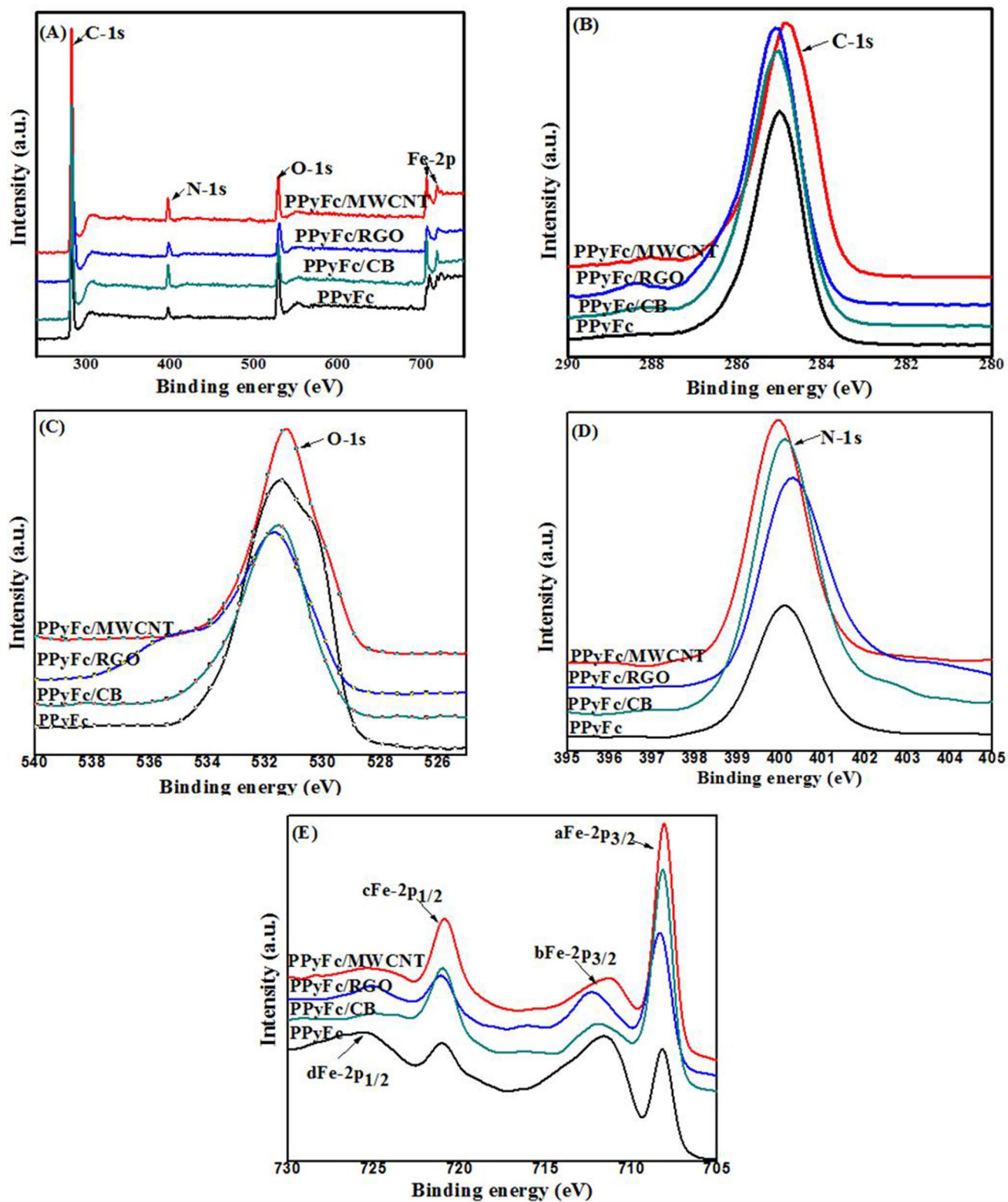


Fig. 9 XPS spectra of PPyFc, PPyFc/MWCNT, PPyFc/RGO and PPyFc/CB a survey, b C-1s, c O-1s, d N-1s and e Fe-2p

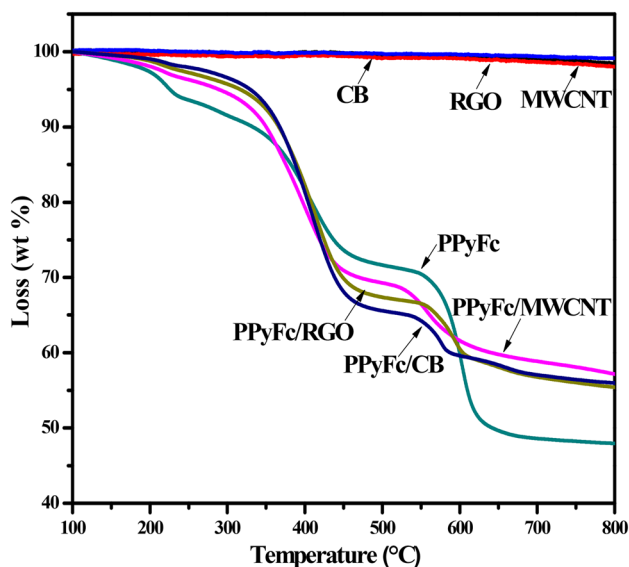


Fig. 10 TGA curves of MWCNT, RGO, CB, PPyFc, PPyFc/MWCNT, PPyFc/RGO and PPyFc/CB

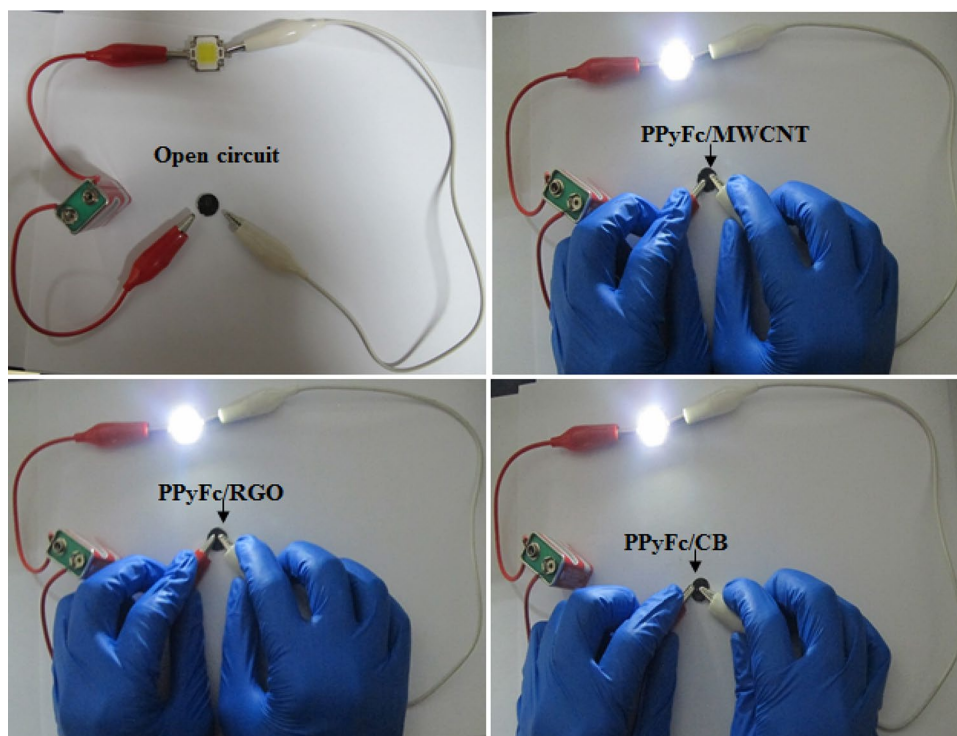
which indicated the presence of PPyFc in the PPyFc/MWCNT, PPyFc/RGO and PPyFc/CB composites.

The information regarding the elemental components of the PPyFc, PPyFc/MWCNT, PPyFc/RGO and PPyFc/CB were determined from the XPS analysis, and the related spectra are presented in Fig. 9.

From the XPS survey spectra as shown in Fig. 9a, the PPyFc, PPyFc/MWCNT, PPyFc/RGO and PPyFc/CB are made up of C, O, N and Fe elements. The binding energy (BE) peaks at around 285 and 532 eV are ascribed to C-1 s and O-1 s, respectively, as shown in Fig. 9b, c [58]. The BE peaks at around 400 eV are ascribed to N-1 s, which is come from the nitrogen of the pyrrole ring, as shown in Fig. 9d [59, 60]. Similarly, the Fe-2p spectra (Fig. 9e) have shown four peaks, two are located at the BE around 708 and 711.5 which are associated to the Fe-2p_{3/2}, whereas the rest of two peaks at the BE around 720.9 and 724.9 eV corresponds to Fe-2p_{1/2} [61, 62], all these peaks of Fe-2p are ascribed to the iron of ferrocene units. The XPS analysis also confirmed that the PPyFc/carbon material composites were successfully prepared.

The TGA curves of the MWCNT, RGO, CB, PPyFc, PPyFc/MWCNT, PPyFc/RGO are shown in Fig. 10. It can be seen that the MWCNT, RGO and CB materials are thermally stable and almost no decomposition has been observed [63, 64]. However, for pure PPyFc, three steps weight loss occurred at different stages. The first weight loss appeared at ~210 °C, which is due to the degradation of ferrocene [65]. Afterward, the second and third weight loss observed at ~350 °C and ~560 °C has been ascribed to the decomposition of the PPyFc chain. The total weight loss in the pure PPyFc is ~50%. Whereas, the PPyFc/MWCNT, PPyFc/RGO and PPyFc/CB composites exhibited a total weight loss of ~40%.

Fig. 11 Photographs to demonstrate the PPyFc/MWCNT, PPyFc/RGO and PPyFc/CB composites containing conductive film circuit with a battery and LED light



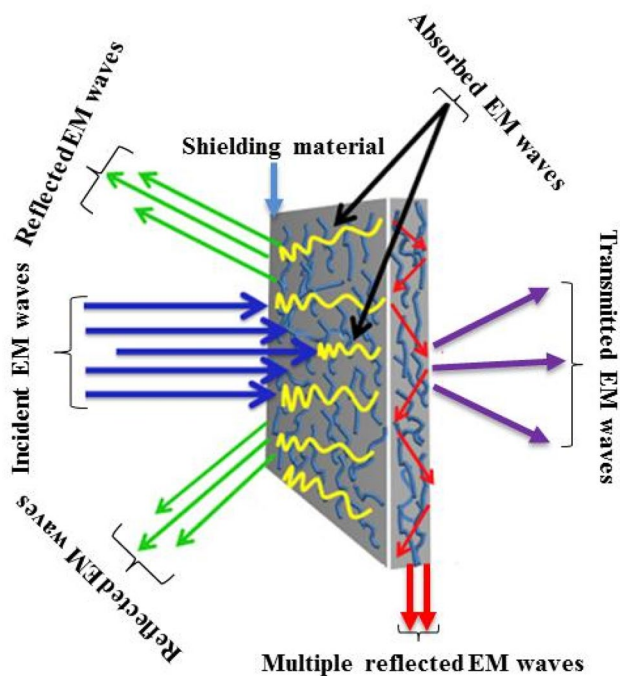


Fig. 12 Schematic illustration showing the possible EMI shielding mechanism [68]

The conductivity of the PPyFc, PPyFc/MWCNT, PPyFc/RGO and PPyFc/CB has been measured using Formula (1) [66]:

$$\text{Conductivity} = \frac{1}{4.53 \times \left(\frac{V}{I}\right) \times d}, \tag{1}$$

where I , V and d are current, voltage and thickness of the film, respectively. The conductivity value of the pure PPyFc is 2.57 S/cm while in the case of PPyFc/CB, PPyFc/RGO and PPyFc/MWCNT composites are 4.64 S/cm, 5.11 S/cm and 7.52 S/cm, respectively, which are more conductive than that of pure PPyFc. The improvement in the electrical conductivity of PPyFc/MWCNT, PPyFc/RGO and PPyFc/CB composites is due to the loading of carbon materials. In addition, we connected the prepared film of the composites to a battery and LED light. As can be seen in Fig. 11, the LED light was off within the open circuit because there was no pathway for the current flow, whereas the LED light was turned on within a closed circuit. These images result indicated that PPyFc/MWCNT, PPyFc/RGO and PPyFc/CB composites are good conductive materials.

3.4 EMI shielding property measurement

The EMI SE is the ability of a material to attenuate EM radiations. It is well known that the EM wave passes in the shielding material such as incident power (P_i) on the shielding material is divided into reflected power (P_r), absorbed power (P_a) and transmitted power (P_t). Therefore, the incident power (P_i) of the shielding material can be described as Formula (2) [67]:

$$P_i = P_r + P_t + P_a. \tag{2}$$

Besides, shielding material controls the radiated EM waves and indicates that less of EM waves are transmitted, but most of them are reflected or absorbed through the shielding material. The general schematic representation of the attenuation of propagated EM waves produced through the shielding material is shown in Fig. 12.

As we know that the total shielding effectiveness (SE_T) mainly consists of three parts, namely, shielding reflection (SE_R), shielding absorption (SE_A) and shielding multiple reflections (SE_{MR}) of the EM radiation and the value of EMI shielding is typically measured in decibel (dB). Even so, the SE_T of the materials can be defined as the sum of SE_R , SE_A and SE_{MR} . Additionally, the SE_T can also be calculated from the logarithm of P_i and P_t ratio of the EM waves. So the SE_T can be expressed as Formula (3) [69]:

$$SE_T(\text{dB}) = SE_R + SE_A + SE_{MR} = 10 \log \left(\frac{P_i}{P_t} \right). \tag{3}$$

The effect of SE_{MR} of the material is negligible when SE of the material is > -10 dB. Hence, SE_T can be expressed as Formula (4) [70]:

$$SE_T(\text{dB}) = SE_R + SE_A. \tag{4}$$

The EMI shielding property of the composites has been measured through the coaxial method and the instrumental setup for measuring EMI SE as shown in Fig. 13.

In EMI shielding, reflection and absorption are the main mechanisms of EM radiations. For the reflection of EM radiations, the materials must have mobile charge carriers, while the absorption of radiations depends on the electric and magnetic dipoles, which interact with the EM field in the radiation. As a result, shielding materials need to be electrically conductive. It is also very important to have good connectivity within the conduction path [71, 72]. In general, when the EMI SE values reached -10 and -20 dB, the material is capable of blocking $\sim 90\%$ and $\sim 99\%$ of the incident EM waves, respectively [73–75]. Figure 14 shows the EMI SE values of PPyFc/CB, PPyFc/RGO and PPyFc/



Fig. 13 EMI SE measurement setup

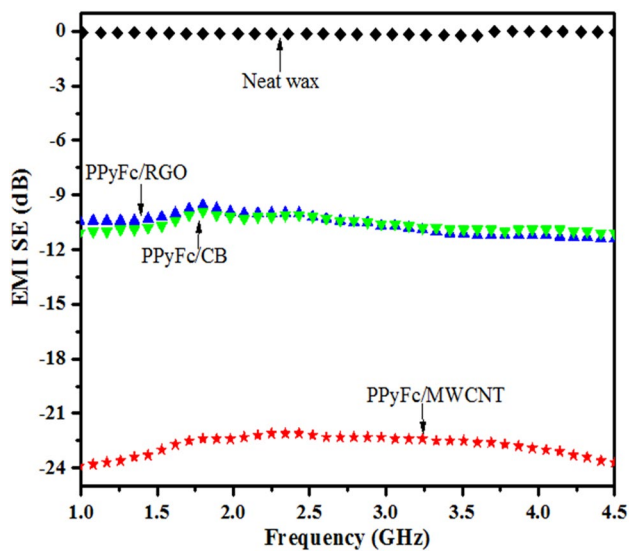


Fig. 14 EMI SE of neat wax, PPyFc/MWCNT, PPyFc/RGO and PPyFc/CB composites in the 1–4.5 GHz

MWCNT composites and achieved -11.08 dB, -11.44 dB and -23.74 dB, respectively.

Furthermore, $\sim 99\%$ attenuation of the EMI radiation was achieved by PPyFc/MWCNT (-23.74 dB). In contrast, $\sim 90\%$ attenuation of the EMI radiation was achieved by PPyFc/RGO (-11.44 dB) and PPyFc/CB (-11.08 dB). In addition, it is also worth noting that there is no EMI SE of neat wax which we used as a support. As we see that the conductive property of the PPyFc/MWCNT, PPyFc/RGO and PPyFc/CB composites increased, which is due to the addition of carbon materials. It means that carbon material as conductive filler played a significant role in improving the conductive pathway of the PPyFc composites which is good for the EMI shielding performance.

4 Conclusion

In this study, PPyFc composites containing MWCNT, RGO and CB were prepared via oxidative polymerization and characterized by SEM, TEM, FTIR, XRD, XPS and TG techniques. The PPyFc/MWCNT, PPyFc/RGO and PPyFc/CB composites showed good electrical conductive properties which were tested by a four-probe method. EMI SE of the PPyFc/MWCNT, PPyFc/RGO and PPyFc/CB composites was measured through a coaxial method in the 1–4.5 GHz. The EMI SE achieved for PPyFc/CB, PPyFc/RGO and PPyFc/MWCNT composites was – 11.08 dB, – 11.44 dB and – 23.74 dB, respectively. Finally, our results suggest that the PPyFc/MWCNT composite is a good shielding material for EMI applications because the achieved EMI SE value (– 23.74 dB) of PPyFc/MWCNT composite corresponds to ~99% attenuation of the incident waves. Furthermore, the PPyFc/MWCNT composite also completed the demand for commercial application (~20 dB). This work provides an easy way to prepare a new generation of eco-friendly and highly efficient EMI shielding materials.

Acknowledgements Financial supports from the National Natural Science Foundation of China (51673170, 51873189 and 51811530097) are gratefully acknowledged.

Compliance with ethical standards

Conflict of interest We declare that we have no financial and personal relationships with other people or organizations that can inappropriately influence our work, the manuscript entitled, “Electromagnetic interference shielding properties of ferrocene-based polypyrrole/carbon material composites”.

References

1. F. Shahzad, S. Yu, P. Kumar, J.W. Lee, Y.H. Kim, S.M. Hong, C.M. Koo, Sulfur doped graphene/polystyrene nanocomposites for electromagnetic interference shielding. *Compos. Struct.* **133**, 1267–1275 (2015)
2. Y.N. Wang, X.D. Cheng, W.L. Song, C.J. Ma, X.M. Bian, M.J. Chen, Hydro-sensitive sandwich structures for self-tunable smart electromagnetic shielding. *Chem. Eng. J.* **344**, 342–352 (2018)
3. Y. Zhan, Z. Long, X. Wan, J. Zhang, S. He, Y. He, 3D carbon fiber mats/nano-Fe₃O₄ hybrid material with high electromagnetic shielding performance. *Appl. Surf. Sci.* **444**, 710–720 (2018)
4. Y. Li, B. Shen, D. Yi, L. Zhang, W. Zhai, X. Wei, W. Zheng, The influence of gradient and sandwich configurations on the electromagnetic interference shielding performance of multilayered thermoplastic polyurethane/graphene composite foams. *Compos. Sci. Technol.* **138**, 209–216 (2017)
5. J. Gonzalez-Rubio, E. Arribas, R. Ramirez-Vazquez, A. Najera, Radiofrequency electromagnetic fields and some cancers of unknown etiology: an ecological study. *Sci. Total Environ.* **599**, 834–843 (2017)
6. K.K. Kesari, A. Agarwal, R. Henkel, Radiations and male fertility. *Reprod. Biol. Endocrinol.* **16**, 118–134 (2018)
7. M.L. Pall, Wi-Fi is an important threat to human health. *Environ. Res.* **164**, 405–416 (2018)
8. A. Nazir, H. Yu, L. Wang, M. Haroon, R.S. Ullah, S. Fahad, K.R. Naveed, T. Elshaarani, A. Khan, M. Usman, Recent progress in the modification of carbon materials and their application in composites for electromagnetic interference shielding. *J. Mater. Sci.* **53**, 8699–8719 (2018)
9. S. Biswas, S.S. Panja, S. Bose, Tailored distribution of nanoparticles in bi-phasic polymeric blends as emerging materials for suppressing electromagnetic radiation: challenges and prospects. *J. Mater. Chem. C* **6**, 3120–3142 (2018)
10. D. Lu, Z. Mo, B. Liang, L. Yang, Z. He, H. Zhu, Z. Tang, X. Gui, Flexible, lightweight carbon nanotube sponges and composites for high-performance electromagnetic interference shielding. *Carbon* **133**, 457–463 (2018)
11. A.V. Menon, G. Madras, S. Bose, Magnetic alloy-MWNT heterostructure as efficient electromagnetic wave suppressors in soft nanocomposites. *ChemistrySelect* **2**, 7831–7844 (2017)
12. S.R. Dhakate, K.M. Subhedar, B.P. Singh, Polymer nanocomposite foam filled with carbon nanomaterials as an efficient electromagnetic interference shielding material. *RSC Adv.* **5**, 43036–43057 (2015)
13. T.K. Gupta, B.P. Singh, R.B. Mathur, S.R. Dhakate, Multi-walled carbon nanotube–graphene–polyaniline multiphase nanocomposite with superior electromagnetic shielding effectiveness. *Nanoscale* **6**, 842–851 (2014)
14. S. Mondal, L. Nayak, M. Rahaman, A. Aldabahi, T.K. Chaki, D. Khastgir, N.C. Das, An effective strategy to enhance mechanical, electrical, and electromagnetic shielding effectiveness of chlorinated polyethylene-carbon nanofiber nanocomposites. *Compos. B Eng.* **109**, 155–169 (2017)
15. S. Mondal, P. Das, S. Ganguly, R. Ravindren, S. Remanan, P. Bhawal, T.K. Das, N.C. Das, Thermal-air ageing treatment on mechanical, electrical, and electromagnetic interference shielding properties of lightweight carbon nanotube based polymer nanocomposites. *Compos. A Appl. Sci. Manuf.* **107**, 447–460 (2018)
16. S.H. Aboutalebi, R. Jalili, D. Esrafilzadeh, M. Salari, Z. Gholamvand, S.A. Yamini, K. Konstantinov, R.L. Shepherd, J. Chen, S.E. Moulton, P.C. Innis, A.I. Minett, J.M. Razal, G.G. Wallace, High-performance multifunctional graphene yarns: toward wearable all-carbon energy storage textiles. *ACS Nano* **8**, 2456–2466 (2014)
17. H. Wang, K. Zheng, X. Zhang, Y.Y. Wang, C. Xiao, L. Chen, X.Y. Tian, Hollow microsphere-infused porous poly(vinylidene fluoride)/multiwall carbon nanotube composites with excellent electromagnetic shielding and low thermal transport. *J. Mater. Sci.* **53**, 6042–6052 (2018)
18. H.Y. Wu, L.C. Jia, D.X. Yan, J.F. Gao, X.P. Zhang, P.G. Ren, Z.M. Li, Simultaneously improved electromagnetic interference shielding and mechanical performance of segregated carbon nanotube/polypropylene composite via solid phase molding. *Compos. Sci. Technol.* **156**, 87–94 (2018)
19. K. Chizari, M. Arjmand, Z. Liu, U. Sundararaj, D. Therriault, Three-dimensional printing of highly conductive polymer nanocomposites for EMI shielding applications. *Mater. Today Commun.* **11**, 112–118 (2017)
20. H. Wang, K. Zheng, X. Zhang, T.X. Du, C. Xiao, X. Ding, C. Bao, L. Chen, X.Y. Tian, Segregated poly(vinylidene fluoride)/MWCNTs composites for high-performance electromagnetic interference shielding. *Compos. A Appl. Sci. Manuf.* **90**, 606–613 (2016)

21. M.H. Al-Saleh, Influence of conductive network structure on the EMI shielding and electrical percolation of carbon nanotube/polymer nanocomposites. *Synth. Methods* **205**, 78–84 (2015)
22. H. Zhang, H. Han, X. Xu, Dynamic and regional constructive electromagnetic protecting materials made by MWNT/Fe₃O₄/poly pyrrole doped vitrimers. *Compos. Sci. Technol.* **158**, 61–66 (2018)
23. C.H. Cui, D.X. Yan, H. Pang, X. Xu, L.C. Jia, Z.M. Li, Formation of a segregated electrically conductive network structure in a low-melt-viscosity polymer for highly efficient electromagnetic interference shielding. *ACS Sustain. Chem. Eng.* **4**, 4137–4145 (2016)
24. R. Bera, S. Paria, S.K. Karan, A.K. Das, A. Maitra, B.B. Khatua, NaCl leached sustainable porous flexible Fe₃O₄ decorated RGO-polyaniline/PVDF composite for durable application against electromagnetic pollution. *Express Polym. Lett.* **11**, 419–433 (2017)
25. B. Shen, Y. Li, D. Yi, W.T. Zhai, X.C. Wei, W.G. Zheng, Strong flexible polymer/graphene composite films with 3D saw-tooth folding for enhanced and tunable electromagnetic shielding. *Carbon* **113**, 55–62 (2017)
26. Y. Wu, Z. Wang, X. Liu, X. Shen, Q. Zheng, Q. Xue, J.K. Kim, Ultralight graphene foam/conductive polymer composites for exceptional electromagnetic interference shielding. *ACS Appl. Mater. Interfaces.* **9**, 9059–9069 (2017)
27. S.C. Tjong, Polymer composites with graphene nanofillers: electrical properties and applications. *J. Nanosci. Nanotechnol.* **14**, 1154–1168 (2014)
28. D.X. Yan, H. Pang, B. Li, R. Vajtai, L. Xu, P.G. Ren, J.H. Wang, Z.M. Li, Structured reduced graphene oxide/polymer composites for ultra-efficient electromagnetic interference shielding. *Adv. Funct. Mater.* **25**, 559–566 (2015)
29. M.H. Al-Saleh, U. Sundararaj, Electromagnetic interference (EMI) shielding effectiveness of PP/PS polymer blends containing high structure carbon black. *Macromol. Mater. Eng.* **293**, 621–630 (2008)
30. C. Merlini, G.M.O. Barra, M.D.P.P. da Cunha, I.D.A.S. Ramoa, B.G. Soares, A. Pegoretti, Electrically conductive composites of polyurethane derived from castor oil with polypyrrole-coated peach palm fibers. *Polym. Compos.* **38**, 2146–2155 (2017)
31. J.M. Thomassin, C. Jérôme, T. Pardoen, C. Bailly, I. Huynen, C. Detrembleur, Polymer/carbon based composites as electromagnetic interference (EMI) shielding materials. *Mater. Sci. Eng. R Rep.* **74**, 211–232 (2013)
32. V.V. Tat'yana, N.E. Oleg, Polypyrrole: a conducting polymer; its synthesis, properties and applications. *Russ. Chem. Rev.* **66**, 443–457 (1997)
33. L.X. Wang, X.G. Li, Y.L. Yang, Preparation, properties and applications of polypyrroles. *React. Funct. Polym.* **47**, 125–139 (2001)
34. P. Sambyal, S.K. Dhawan, P. Gairola, S.S. Chauhan, S.P. Gairola, Synergistic effect of polypyrrole/BST/RGO/Fe₃O₄ composite for enhanced microwave absorption and EMI shielding in X-Band. *Curr. Appl. Phys.* **18**, 611–618 (2018)
35. Y. Wang, F.Q. Gu, L.J. Ni, K. Liang, K. Marcus, S.L. Liu, F. Yang, J.J. Chen, Z.S. Feng, Easily fabricated and lightweight PPy/PDA/AgNW composites for excellent electromagnetic interference shielding. *Nanoscale* **9**, 18318–18325 (2017)
36. A.A.J. Torriero, Characterization of decamethylferrocene and ferrocene in ionic liquids: argon and vacuum effect on their electrochemical properties. *Electrochim. Acta* **137**, 235–244 (2014)
37. P.J. Chirik, Expanding the boundaries of organometallic chemistry. *Organometallics* **37**, 835–836 (2018)
38. A. Abd-El-Aziz, E.K. Todd, R.M. Okasha, T.H. Afifi, Organonion polymers containing azo dyes. *Macromol. Symp.* **196**, 89–99 (2003)
39. Z. Bicil, P. Camurlu, B. Yucel, B. Becer, Multichromic, ferrocene clicked poly(2,5-dithienylpyrrole)s. *J. Polym. Res.* **20**, 228–234 (2013)
40. H. Qin, T. Gong, Y. Cho, C. Lee, T. Kim, A conductive copolymer of graphene oxide/poly(1-(3-aminopropyl)pyrrole) and the adsorption of metal ions. *Polym. Chem.* **5**, 4466–4473 (2014)
41. S. Radhakrishnan, S. Paul, Conducting polypyrrole modified with ferrocene for applications in carbon monoxide sensors. *Sens. Actuators B Chem.* **125**, 60–65 (2007)
42. H. Kato, O. Nishikawa, T. Matsui, S. Honma, H. Kokado, Fourier-transform infrared-spectroscopy study of conducting polymer polypyrrole higher order structure of electrochemically synthesized film. *J. Phys. Chem.* **95**, 6014–6016 (1991)
43. F. Andreani, L. Angiolini, V. Greci, E. Salatelli, Optically active polyalkylthiophenes: synthesis and polymerization of chiral, symmetrically substituted, quinquethiophene monomer. *Synth. Methods* **145**, 221–227 (2004)
44. S. Goel, N.A. Mazumdar, A. Gupta, Synthesis and characterization of polypyrrole nanofibers with different dopants. *Polym. Adv. Technol.* **21**, 205–210 (2010)
45. S. Gurunathan, J.W. Han, E.S. Kim, J.H. Park, J.H. Kim, Reduction of graphene oxide by resveratrol: a novel and simple biological method for the synthesis of an effective anticancer nanotherapeutic molecule. *Int. J. Nanomed.* **10**, 2951–2969 (2015)
46. C. Cunha, S. Panseri, D. Iannazzo, A. Piperno, A. Pistone, M. Fazio, A. Russo, M. Marcacci, S. Galvagno, Hybrid composites made of multiwalled carbon nanotubes functionalized with Fe₃O₄ nanoparticles for tissue engineering applications. *Nanotechnology* **23**, 465102–465112 (2012)
47. C.D. Zappiello, D.M. Nanicuacua, W.N.L. dos Santos, D.L.F. da Silva, L.H. Dall'Antonia, F.M. de Oliveira, D.N. Clausen, C.R.T. Tarley, Solid phase extraction to on-line preconcentrate trace cadmium using chemically modified nano-carbon black with 3-mercaptopropyltrimethoxysilane. *J. Braz. Chem. Soc.* **27**, 1715–1726 (2016)
48. B. Yeole, T. Sen, D.P. Hansora, S. Mishra, Effect of electrical properties on gas sensitivity of polypyrrole/cds nanocomposites. *J. Appl. Polym. Sci.* **132**, 42379–42388 (2015)
49. X. Liu, D. Shou, C. Chen, H. Mao, Y. Kong, Y. Tao, Core-shell structured polypyrrole/mesoporous SiO₂ nanocomposite capped with graphene quantum dots as gatekeeper for irradiation-controlled release of methotrexate. *Mater. Sci. Eng. C Mater. Biol. Appl.* **81**, 206–212 (2017)
50. C. Su, L. Wang, L. Xu, C. Zhang, Synthesis of a novel ferrocene-contained polypyrrole derivative and its performance as a cathode material for Li-ion batteries. *Electrochim. Acta* **104**, 302–307 (2013)
51. A. Hassanein, N. Salahuddin, A. Matsuda, G. Kawamura, M. Elfiky, Fabrication of biosensor based on chitosan-ZnO/polypyrrole nanocomposite modified carbon paste electrode for electro-analytical application. *Mater. Sci. Eng. C Mater. Biol. Appl.* **80**, 494–501 (2017)
52. B. Tian, G. Zerbi, Lattice dynamics and vibrational spectra of polypyrrole. *J. Chem. Phys.* **92**, 3886–3891 (1990)
53. S.T. Navale, A.T. Mane, M.A. Chougule, R.D. Sakhare, S.R. Nalage, V.B. Patil, Highly selective and sensitive room temperature NO₂ gas sensor based on polypyrrole thin films. *Synth. Methods* **189**, 94–99 (2014)
54. R. Atchudan, J. Joo, A. Pandurangan, An efficient synthesis of graphenated carbon nanotubes over the tailored mesoporous molecular sieves by chemical vapor deposition. *Mater. Res. Bull.* **48**, 2205–2212 (2013)
55. J. Sun, X. Shu, Y. Tian, Z. Tong, S. Bai, R. Luo, D. Li, C.C. Liu, Facile preparation of polypyrrole-reduced graphene oxide hybrid for enhancing NH₃ sensing at room temperature. *Sens. Actuators B Chem.* **241**, 658–664 (2017)

56. T. Ungar, J. Gubicza, G. Ribarik, C. Pantea, T.W. Zerda, Micro-structure of carbon blacks determined by X-ray diffraction profile analysis. *Carbon* **40**, 929–937 (2002)
57. F. Kanwal, S.A. Siddiqi, A. Batool, M. Imran, W. Mushtaq, T. Jamil, Synthesis of polypyrrole–ferric oxide (Ppy–Fe₂O₃) composites and study of their structural and conducting properties. *Synth. Methods* **161**, 335–339 (2011)
58. A.K. Thakur, R.B. Choudhary, M. Majumder, G. Gupta, In-situ integration of waste coconut shell derived activated carbon/polypyrrole/rare earth metal oxide (Eu₂O₃): a novel step towards ultrahigh volumetric capacitance. *Electrochim. Acta* **251**, 532–545 (2017)
59. A. Morozan, P. Jegou, S. Campidelli, S. Palacin, B. Jusselme, Relationship between polypyrrole morphology and electrochemical activity towards oxygen reduction reaction. *Chem. Commun.* **48**, 4627–4629 (2012)
60. P. Pfluger, G.B. Street, Chemical electronic and structural properties of conducting heterocyclic polymers—a view by XPS. *J. Chem. Phys.* **80**, 544–553 (1984)
61. C.M. Woodbridge, D.L. Pugmire, R.C. Johnson, N.M. Boag, M.A. Langell, HREELS and XPS studies of ferrocene on Ag(100). *J. Phys. Chem. B* **104**, 3085–3093 (2000)
62. Q. Dong, X. Zhuang, Z. Li, B. Li, B. Fang, C. Yang, H. Xie, F. Zhang, X. Feng, Efficient approach to iron/nitrogen co-doped graphene materials as efficient electrochemical catalysts for the oxygen reduction reaction. *J. Mater. Chem. A* **3**, 7767–7772 (2015)
63. M. Mishra, A.P. Singh, V. Gupta, A. Chandra, S.K. Dhawan, Tunable EMI shielding effectiveness using new exotic carbon: polymer composites. *J. Alloy. Compd.* **688**, 399–403 (2016)
64. C.M. Wong, D.B. Walker, A.H. Soeriyadi, J.J. Gooding, B.A. Messerle, A versatile method for the preparation of carbon–rhodium hybrid catalysts on graphene and carbon black. *Chem. Sci.* **7**, 1996–2004 (2016)
65. A.C. de Souza, A.T.N. Pires, V. Soldi, Thermal stability of ferrocene derivatives and ferrocene-containing polyamides. *J. Therm. Anal. Calorim.* **70**, 405–414 (2002)
66. M. Jana, S. Saha, P. Khanra, P. Samanta, H. Koo, N. Chandra Murmu, T. Kuila, Non-covalent functionalization of reduced graphene oxide using sulfanilic acid azocromotrop and its application as a supercapacitor electrode material. *J. Mater. Chem. A* **3**, 7323–7331 (2015)
67. R. Bera, S. Suin, S. Maiti, N.K. Shrivastava, B.B. Khatua, Carbon nanohorn and graphene nanoplate based polystyrene nanocomposites for superior electromagnetic interference shielding applications. *J. Appl. Polym. Sci.* **132**, 42803–42817 (2015)
68. M.H. Al-Saleh, U. Sundararaj, Electromagnetic interference shielding mechanisms of CNT/polymer composites. *Carbon* **47**, 1738–1746 (2009)
69. P. Saini, V. Choudhary, B.P. Singh, R.B. Mathur, S.K. Dhawan, Polyaniline–MWCNT nanocomposites for microwave absorption and EMI shielding. *Mater. Chem. Phys.* **113**, 919–926 (2009)
70. S.T. Hsiao, C.C.M. Ma, H.W. Tien, W.H. Liao, Y.S. Wang, S.M. Li, C.Y. Yang, S.C. Lin, R.B. Yang, Effect of covalent modification of graphene nanosheets on the electrical property and electromagnetic interference shielding performance of a waterborne polyurethane composite. *ACS Appl. Mater. Interfaces.* **7**, 2817–2826 (2015)
71. X. Mei, L. Lu, Y. Xie, W. Wang, Y. Tang, K.S. Teh, An ultrathin carbon-fabric/graphene/poly(vinylidene fluoride) film for enhanced electromagnetic interference shielding. *Nanoscale* **11**, 13587–13599 (2019)
72. D. Xing, L. Lu, K.S. Teh, Z. Wan, Y. Xie, Y. Tang, Highly flexible and ultra-thin Ni-plated carbon-fabric/polycarbonate film for enhanced electromagnetic interference shielding. *Carbon* **132**, 32–41 (2018)
73. B. Zhao, C.X. Zhao, R.S. Li, S.M. Hamidinejad, C.B. Park, Flexible, ultrathin, and high-efficiency electromagnetic shielding properties of poly(vinylidene fluoride)/carbon composite films. *ACS Appl. Mater. Interfaces.* **9**, 20873–20884 (2017)
74. B. Zhao, G. Shao, B. Fan, W. Zhao, Y. Xie, R. Zhang, Facile preparation and enhanced microwave absorption properties of core-shell composite spheres composed of Ni cores and TiO₂ shells. *Phys. Chem. Chem. Phys.* **17**, 8802–8810 (2015)
75. J. Anupama, B. Anil, S. Rajvinder, P.S. Alegaonkar, K. Balasubramanian, D. Suwarna, Graphene nanoribbon–PVA composite as EMI shielding material in the X band. *Nanotechnology* **24**, 455705–455713 (2013)

Publisher's Note Springer Nature remains neutral with regard to jurisdictional claims in published maps and institutional affiliations.